Original Article

MOLECULAR METABOLISM

Adipocyte-specific *Nos2* deletion improves insulin resistance and dyslipidemia through brown fat activation in diet-induced obese mice

Vanessa Rodrigues Vilela [1,4], Nolwenn Samson [1,4], Renato Nachbar [1], Lia Rossi Perazza [1], Gabriel Lachance [1], Volatiana Rokatoarivelo [1], Carolina Centano-Baez [1], Patricia Zancan [1,5], Mauro Sola-Penna [1,5], Kerstin Bellmann [1], Vincenzo Di Marzo [1,2,3], Mathieu Laplante [1], André Marette [1,2,*]

ABSTRACT

Objective: Inducible nitric oxide (NO) synthase (NOS2) is a well-documented inflammatory mediator of insulin resistance in obesity. NOS2 expression is induced in both adipocytes and macrophages within adipose tissue during high-fat (HF)-induced obesity.

Methods: Eight-week-old male mice with adipocyte selective deletion of the *Nos2* gene ($Nos2^{AD-KO}$) and their wildtype littermates ($Nos2^{fl/fl}$) were subjected to chow or high-fat high-sucrose (HFHS) diet for 10 weeks followed by metabolic phenotyping and determination of brown adipose tissue (BAT) thermogenesis. The direct impact of NO on BAT mitochondrial respiration was also assessed in brown adipocytes.

Results: HFHS-fed $Nos2^{AD-KO}$ mice had improved insulin sensitivity as compared to $Nos2^{fl/fl}$ littermates. $Nos2^{AD-KO}$ mice were also protected from HF-induced dyslipidemia and exhibited increased energy expenditure compared with $Nos2^{fl/fl}$ mice. This was linked to the activation of BAT in HFHS-fed $Nos2^{AD-KO}$ mice as shown by increased *Ucp1* and *Ucp2* gene expression and augmented respiratory capacity of BAT mitochondria. Furthermore, mitochondrial respiration was inhibited by NO, or upon cytokine-induced NOS2 activation, but improved by NOS2 inhibition in brown adipocytes.

Conclusions: These results demonstrate the key role of adipocyte NOS2 in the development of obesity-linked insulin resistance and dyslipidemia, partly through NO-dependent inhibition of BAT mitochondrial bioenergetics.

© 2022 The Authors. Published by Elsevier GmbH. This is an open access article under the CC BY-NC-ND license (http://creativecommons.org/licenses/by-nc-nd/4.0/).

Keywords Nitric oxide synthase; Dyslipidemia; Obesity; Insulin resistance; brown adipose tissue; Mitochondrial respiration

1. INTRODUCTION

Nitric oxide (NO) is synthesized by nitric oxide synthase enzymes (NOS). The inducible member of the NOS family, NOS2 (formerly iNOS), is activated in response to bacterial endotoxins, cytokines, and nutrient overload [1]. NOS2 can produce large amounts of NO over prolonged periods of time and plays a key role in host defense through its bacteriostatic action [2]. However, NOS2 is also a key mediator of inflammation and insulin resistance, and chronic NOS2 induction in obesity interferes with insulin signaling to phosphatidylinositol 3-kinase PI3K (PI3K)/Akt in metabolic tissues [3,4]. NOS2 expression is also associated with type 2 diabetes in humans [5,6]. Genetic invalidation of *Nos2* protects mice from insulin resistance mediated by obesity, lipid infusion, and lipopolysaccharide (LPS) challenge [4,7–9]. NOS2 is induced in all metabolic tissues during obesity [7,8,10,11] and mostly found in macrophages in adipose tissue [12]. However, myeloid *Nos2* depletion did not protect mice from insulin resistance, whereas pharmacological NOS2 inhibition improved insulin action in HF-fed mice [13]. These results suggest that NOS2 expression in metabolic cells is key to disrupt metabolic homeostasis in obesity. To directly test this hypothesis, we generated mice with adipose-specific *Nos2* deletion using Cre/loxP recombination. Interestingly, these mice showed improved insulin sensitivity and lipid profile upon HFHS feeding, which were associated with brown adipose tissue (BAT) activation. We further showed using cultured BAT cells that NOS2 activation can directly inhibit mitochondrial oxidative metabolism.

2. METHODS

2.1. Animals and genotyping

Mice containing flox sites spanning Exon 2 of *Nos2* were created (Ingenious, Stony Brook, NY, USA), crossed with B6.Cg-Tg (ACT FLPe)

[1]Quebec Heart & Lung Institute, Université Laval, 2725 Ch Ste-Foy, Québec, QC, G1V 4G5, Canada [2]Institute of Nutrition and Functional Foods, Centre NUTRISS, Université Laval, 2440 Boulevard Hochelaga Suite 1710, Québec, QC, G1V 0A6, Canada [3]Canada Excellence Research Chair Microbiome-Endocannabinoidome Axis in Metabolic Health (CERC-MEND), Canada

[4] Vanessa Rodrigues Vilela and Nolwenn Samson contributed equally to this work.
[5] Present address: Department of Pharmaceutical Biotechnology, Federal University of Rio de Janeiro, Rio de Janeiro, RJ, 21941-902, Brazil.

*Corresponding author. The Quebec Heart and Lung Institute, Hôpital Laval, Pavillon Marguerite d'Youville Bureau Y4340, Ste-Foy, Québec, G1V 4G5, Canada. E-mail: andre.marette@criucpq.ulaval.ca (A. Marette).

Received May 20, 2021 • Revision received December 22, 2021 • Accepted January 3, 2022 • Available online 14 January 2022

https://doi.org/10.1016/j.molmet.2022.101437

 © 2022 The Authors. Published by Elsevier GmbH. This is an open access article under the CC BY-NC-ND license (http://creativecommons.org/licenses/by-nc-nd/4.0/).

9205Dym/J mice (Jackson Laboratory, Bar Habor, ME, USA) to remove the neomycin cassette and then backcrossed for at least 12 generations on C57BL/6J background (stock No. 000664, Jackson Laboratories). Adipocyte-specific (*Nos2*$^{AD-KO}$) *Nos2* knockout mice were generated by crossing floxed *Nos2* (*Nos2*$^{fl/fl}$) mice with *Adipoq-Cre* (kindly provided by E. Rosen and backcrossed for at least 10 generations on C57BL/6J background). Genomic DNA was extracted from samples using the DNA REDExtract-N-Amp PCR kit (Sigma), and genotyping was performed for floxed *Nos2* and *Adipoq-Cre*. Primers used for floxed *Nos2* were 5'-ggC ACC TAA gAgA gTCT ggT CT CC-3' and 5'-CTG AGG ATA GTA GAG GGC CA TC-3'. Adipoq-Cre-specific recombination of *Nos2* exon 2 was detected by PCR using primers binding to intron 1 (5'-CTTGGCTCAGGATGCGTGAT-3' (forward)) and intron 2 (5'-TTGACACCCTTCAGTTGCCTAA-3' (reverse)) genomic DNA outside of the floxed *Nos2* sites. Genomic DNA was isolated from mouse tissues. Mapping of the recombined alleles was done by directly cloning PCR products into pGEM-T-easy vector (Promega #A1360) followed by T7p DNA sequencing (Genotyping and Sequencing platform, CHU de Québec-Université Laval Research Center). To determine *Nos2* ablation in the adipocyte compartment of white (eWAT, iWAT) and brown (BAT) adipose tissues, mice were injected with LPS (3 mg/kg; i.p.) or saline for 6 h to acutely induce *Nos2* expression. Adipose depots were rapidly removed, cleaned of extraneous tissues, and adipocytes were isolated by collagenase digestion (type II collagenase; Sigma). Floated adipocytes were processed for RNA isolation and qPCR determination of *Nos2* mRNA.

All animal handling and treatments were approved and followed the guidelines set by Laval University Animal Care Ethics Committee and in accordance with the ARRIVE guidelines. Seven-week-old mice bred at our in-house colony at Laval Hospital were transferred to the animal facility of the Institute of Nutritional and Functional foods (Québec, Canada) and housed 1 per cage (12 h daylight cycle, lights off at 18:00) at 22 °C with food and water *ad libitum*. After one week of acclimatization, mice were randomly allocated to standard chow diet or to a HFHS-diet (65% fat, 15% protein, 20% carbohydrates) for 10 weeks. Littermates were used for all the experiments. Body weight gain and food intake were assessed twice weekly. At 10 weeks on diet, animals were anesthetized in chambers saturated with isoflurane and then sacrificed by cardiac puncture. Organs and tissues were collected, and blood was drawn in tubes containing 2 IU of heparin and immediately centrifuged to separate plasma from cells. All interventions were carried out during the animals' light cycle.

2.2. Indirect calorimetry and body composition determinations

Seven weeks into the dietary protocol, mice were individually placed into metabolic cages at thermoneutrality (28 °C) to determine oxygen consumption (VO_2), carbon dioxide production (VCO_2), and the respiratory quotient by indirect calorimetry. Animals were initially placed in their individual metabolic cage for 24 h before the beginning of the experiment. Measurements were made continuously during the following 2 days (36 measurements · mouse^{-1} · day^{-1}) in an Oxymax CLAMS system (Columbus Instruments, Columbus, OH, USA). Data presented are the average of all measurements made over 2 days of monitoring. Body composition was measured by nuclear magnetic resonance with a Bruker Minispec (LF90) apparatus.

2.3. Metabolic measurements

Insulin tolerance was determined in 6-h-fasted mice after 8 weeks on diet. Insulin (0.65 U/kg BW) was injected intraperitoneally before blood collection via the saphenous vein at 0, 5, 10, 15, 20, 30, and 60 min. For glucose tolerance tests (performed 10 weeks post-diet treatment), 12-h-fasted mice were given glucose (1 g of glucose/kg body weight) by gavage, and blood was drawn from the saphenous vein at 0, 15, 30, 60, 90, and 120 min. Additionally, blood samples (∼30 μL) were collected at each time point during oGTT for the determination of insulin concentration.

2.4. Blood metabolite measurements

Blood glucose was measured by glucometer (Accu-Chek). Plasma insulin was measured using ultrasensitive ELISA kit (Alpco, Salem, USA); C-peptide was determined using ELISA kit (Crystal Chem, Elk Grove Village, USA). Plasma triglyceride (TG) (Randox Laboratories, Crumlin, UK), non-esterified fatty-acids (NEFA) (Wako Chemicals, Richmond, VA), cholesterol (Randox Laboratories, Crumlin, UK) and free glycerol levels (Sigma—Aldrich) were enzymatically determined according to the manufacturer's instructions.

2.5. Measurement of plasma and tissue nitrite and nitrate

Nitrite and nitrate levels in plasma, epididymal and inguinal adipose tissue were measured by fluorometric spectrophotometry after reducing nitrate to nitrite using nitrite reductase and the NAHD regenerating system [14]. Briefly, blood was collected in tubes containing EDTA and centrifuged for 10 min at 3200 × *g* to obtain plasma. Tissues were grounded in liquid nitrogen using a pestle and mortar. The tissue powder was resuspended in 5 volumes of Tris buffer (20 mM Tris pH 7.5). Tissue lysates were centrifuged at 2800 × *g* for 20 min and protein concentration of the supernatant was measured by the BCA™ protein assay (Thermo Scientific, Illinois, USA). Plasma and tissue lysates were then centrifuged at 5000 × *g* (4 °C) in an Ultrafree-Microcentrifuge 10000 NMWL filter unit. Fluorescence was measured at λ_{ex} 360 nm and λ_{em} 450 nm.

2.6. Protein extraction and western blotting

Fifty milligram of brown adipose was pulverized with a pestle and mortar in liquid nitrogen, and the powder was homogenized in 4 vol of homogenization buffer (20 mM Tris—HCl pH 7.5, 150 mM NaCl, 1 mM $CaCl_2$, 1 mM $MgCl_2$, 10% glycerol, 1% Igepal CA-630, 10 mM NaF, 2 mM Na_3VO_4, 1 mM PMSF, and protease inhibitors). For western blot analysis, crude protein lysates were solubilized in sample buffer and loaded onto a 6% acrylamide gel and subjected to SDS-PAGE, transferred to nitrocellulose membrane. Non-specific binding sites were blocked with 3% (w/v) dry nonfat milk in TBS-T (100 mM Tris, 1.5 mM NaCl, pH 8.0 and 0.5% Tween 20) and the membrane was incubated overnight with antibodies against mitochondrial complexes I to V (Abcam, #110413, dilution 1:1000). Secondary antibodies were purchased from Jackson Immuno Research Laboratories and diluted 1:10000. The substrate (WBKLS0500, Millipore) was used to image the blots. Bands were detected and recorded using a Bio-Rad Gel Doc 2000 gel documentation system (Bio-Rad, Hercules, CA, USA). Densitometric analysis was conducted using ImageJ software from the National Institutes of Health.

2.7. RNA analysis

Total RNA was isolated using TRIzol reagent (Thermo Fisher Scientific) and total RNA purification was performed using a RNeasy mini kit (Qiagen). Total RNA was used for reversed transcription using High-Capacity cDNA Reverse Transcription Kit (Thermo Fisher Scientific) and cDNA levels were measured by quantitative PCR as described before (27) or by qPCR-based TaqMan® open array (ThermoFisher). Primers are listed in Supplementary Tables 3 and 4

 © 2022 The Authors. Published by Elsevier GmbH. This is an open access article under the CC BY-NC-ND license (http://creativecommons.org/licenses/by-nc-nd/4.0/).

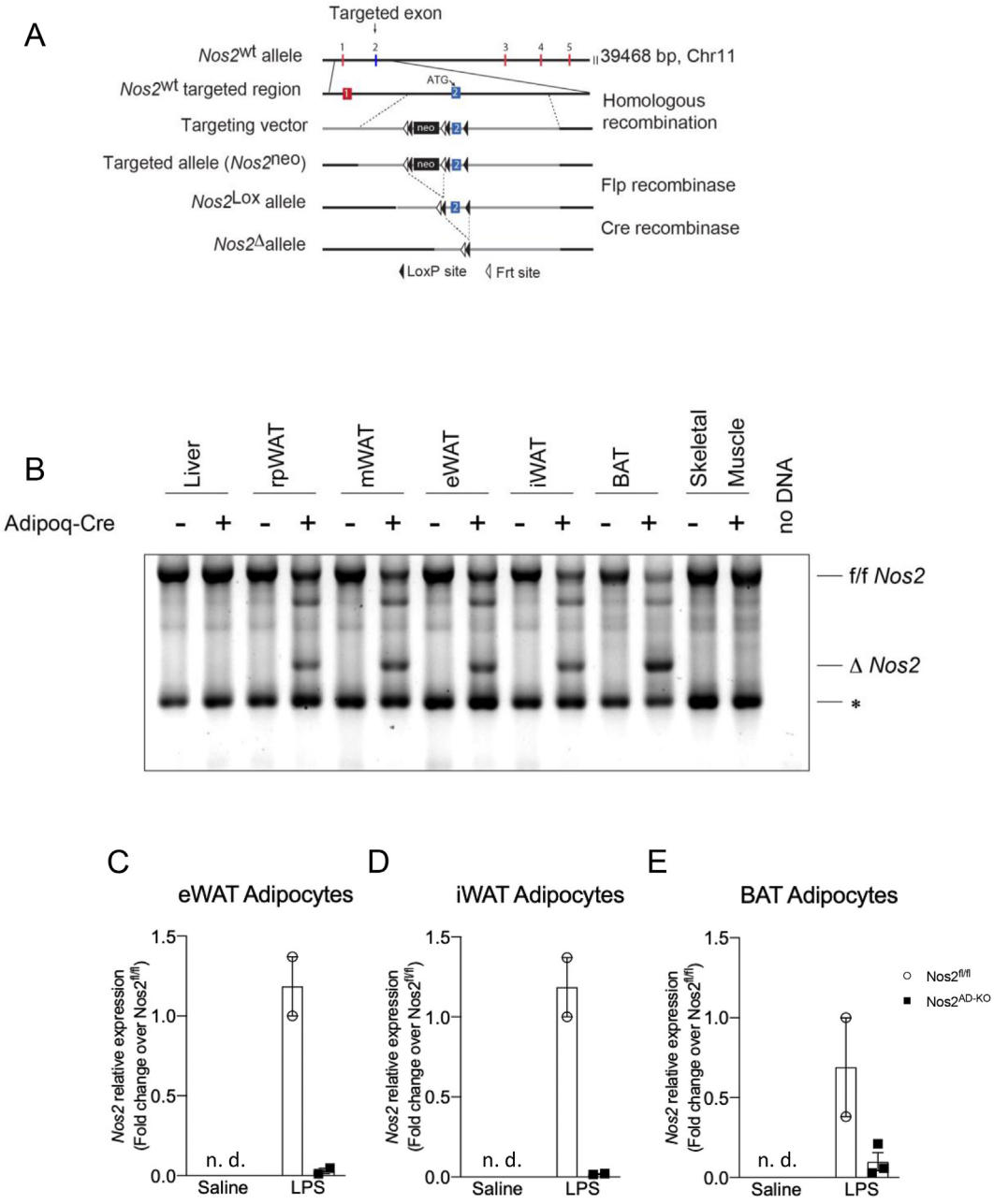

Figure 1: Determination of selective disruption of *Nos2* in adipose tissue. Mice containing flox sites before and after Exon 2 of *Nos2* were created and backcrossed for at least 10 generations on a C57BL/6J background. Adipocyte-specific (*Nos2*$^{AD-KO}$) *Nos2* knockout mice were generated on a C57BL/6J background by crossing mice homozygous for floxed *Nos2* (*Nos2*$^{fl/fl}$) with *Adipoq-Cre* mice (A). Recombined alleles from genomic DNA isolation (B). *unspecific band. Δ: deletion. *Nos2* expression in adipocytes isolated from epididymal (C), inguinal (D) and brown (E) adipose tissue of saline- and LPS-injected mice; N = 2–3.

2.8. Cell culture

T37i cells were cultured in DMEM/Ham's F12 medium supplemented with glutamine (2 mM), Hepes (15 mM) and FBS (10%). Confluent cells were differentiated for 7 days in the presence of insulin (20 nM) and triiodothyronine (2 nM).

2.9. Oxygen consumption

Differentiated T37i cells were seeded in Seahorse 24 well plate at a density of 40000/well and treated for 24 h with a cytokine cocktail (625 U/ml IFNγ, 2.5 ng IL-1β, 0.625 ng/ml TNFα) with or without 1400W (100 μM). After washing the cells thrice with Seahorse XF Medium (DMEM w/o phenol red supplemented with pyruvate (1 mM), glutamine (2 mM) and glucose (10 mM)), the Seahorse mitostress protocol was run. Oxygen consumption was monitored by sequential addition of Oligomycin (1.5 μM), FCCP (1.5 μM), Rotenone (1 μM) and Antimycin A (1 μM). Oligomycin inhibits the activity of the ATP synthase (complex V) and provides information about the ATP-linked cellular respiration. FCCP triggers the disruption of the mitochondrial membrane potential. Under this condition, the cells can reach their maximal oxygen consumption through complex IV. Finally, the addition of Rotenone and Antimycin A, which inhibit the complex I and III, respectively, shuts down mitochondrial respiration to determine non-mitochondrial

 © 2022 The Authors. Published by Elsevier GmbH. This is an open access article under the CC BY-NC-ND license (http://creativecommons.org/licenses/by-nc-nd/4.0/).

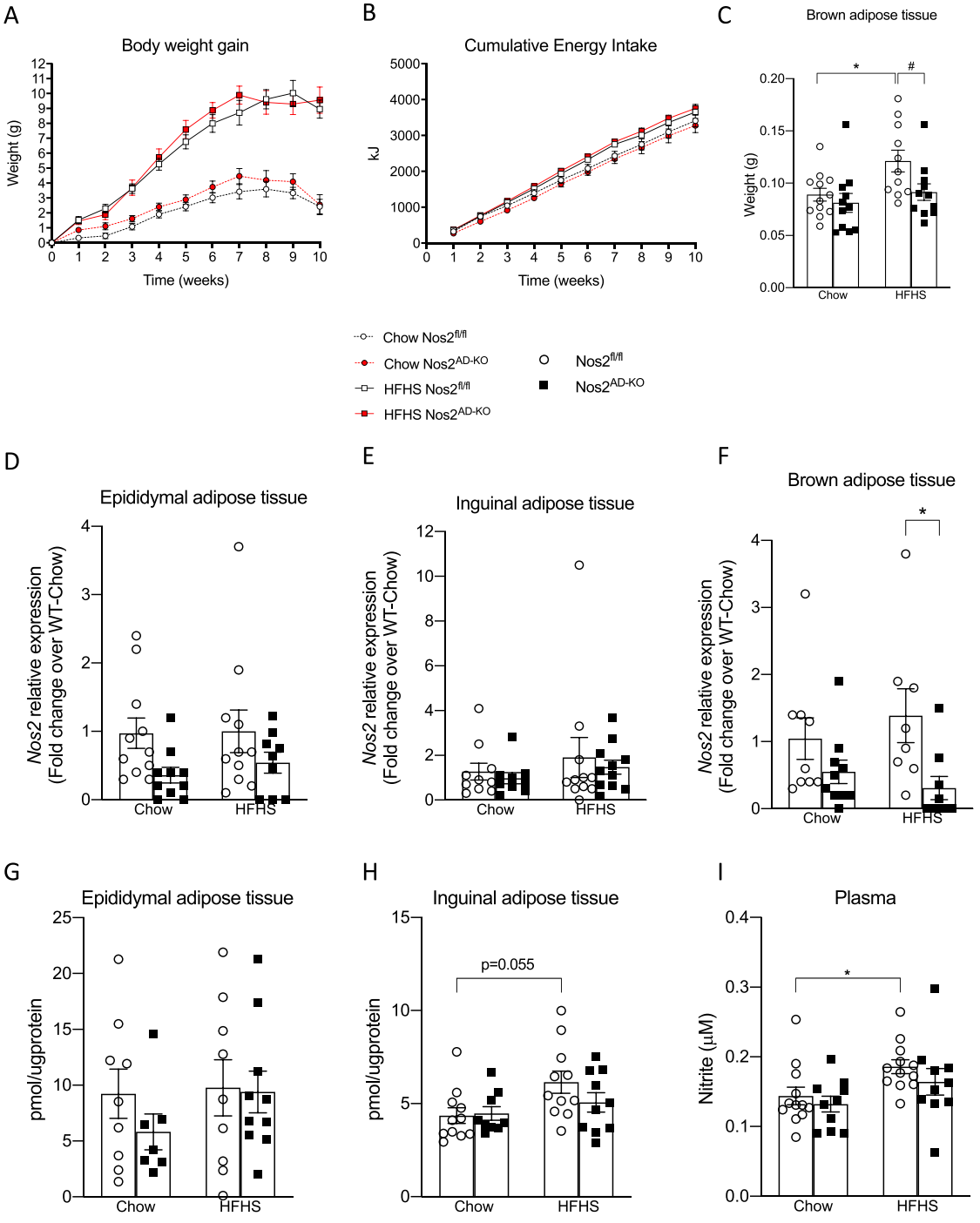

Figure 2: *Nos2*$^{AD-KO}$ prevents HFHS diet increase in brown adipose tissue mass irrespectively of body weight gain. *Nos2*$^{AD-KO}$ mice and wild-type (*Nos2*$^{fl/fl}$) mice were fed either a chow or a high-fat/high sucrose (HFHS) diet for 10 weeks. Total weight gain (A), total energy intake during 10 weeks (B), weight of brown adipose tissue (interscapular) (C). *Nos2* mRNA expression in epididymal (D), inguinal (E) and brown (F) adipose tissue. Nitrite/nitrate content in epididymal (C), inguinal (D) adipose tissue and plasma (E). n = 11−12 mice/group. Two-way ANOVA with a Student-Newman-Keuls post hoc test was applied to calculate the significance of the differences between groups. Data are expressed as the mean ± SEM. ***$p < 0.001$ for diet effect and $^{\#}p < 0.05$ for genotype difference.

 © 2022 The Authors. Published by Elsevier GmbH. This is an open access article under the CC BY-NC-ND license (http://creativecommons.org/licenses/by-nc-nd/4.0/).

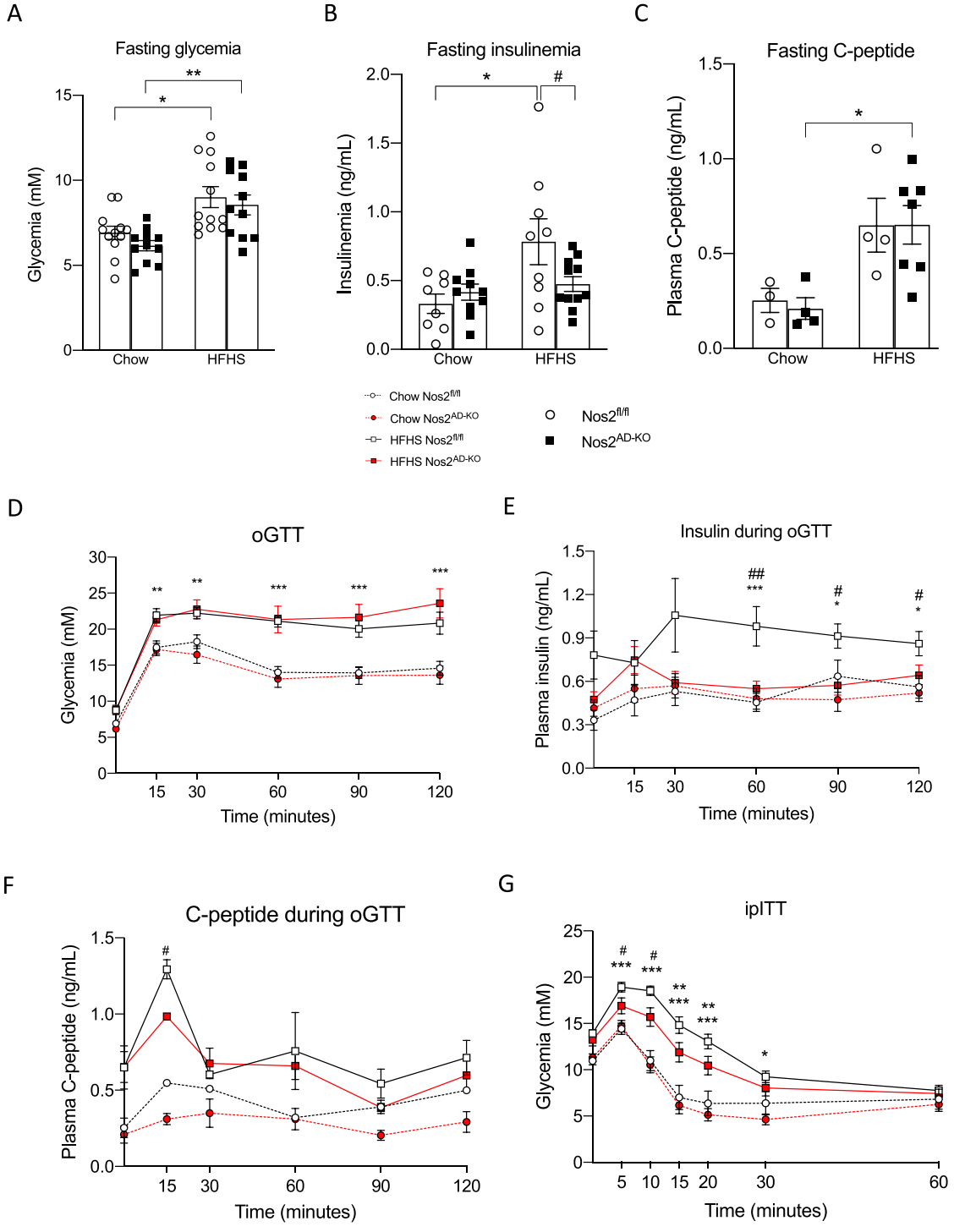

Figure 3: Adipocyte-specific knockout of *Nos2* increases insulin sensitivity and alleviates diet-induced hyperinsulinaemia in HFHS-fed mice. 12 h fasting glycemia (A), insulinemia (B) and C-peptide (C). Mice 10 wk on HFHS diet were fasted overnight (12 h) and an oral glucose tolerance test (D) was performed after gavage with glucose (1 g/kg body weight). Blood samples were collected at each time point during OGTT for insulinaemia and C-peptide determination (E, F). Mice 8 wk on HFHS diet were 6 h fasted and an insulin tolerance test (E) was performed after an intraperitoneal injection of insulin (0.65 UI/kg body weight). n = 11–12 (A, D, E); n = 8–11 (B); n = 7–11 (G), n = 3–6 (C, F). Two-way ANOVA with a Student-Newman-Keuls post hoc test was applied to calculate the significance of the differences between groups. Data are expressed as the mean ± SEM. $^{*}p < 0.05$, $^{**}p < 0.01$ and $^{***}p < 0.001$ for diet effect; $^{\#}p < 0.05$ and $^{\#\#}p < 0.01$ for genotype difference. HFHS, high fat/high sucrose; oGTT, oral glucose tolerance test; ipITT, intraperitoneal insulin tolerance test.

 © 2022 The Authors. Published by Elsevier GmbH. This is an open access article under the CC BY-NC-ND license (http://creativecommons.org/licenses/by-nc-nd/4.0/).

respiration. The OCR measurements were normalized to total DNA content.

2.10. Statistical analysis

All data are presented as means ± SEM. Two-way ANOVA with a Student-Newman-Keuls post hoc test was used to assign significance to the comparisons between groups (GraphPad Software 7, La Jolla, CA, USA). All results were considered statistically significant at $P < 0.05$.

3. RESULTS

3.1. Adipocyte-specific ablation of *Nos2* reduces HFHS diet-induced brown adipose tissue mass

To determine the specific role of NOS2 in adipose tissue, we generated adipocyte-specific (*Nos2*$^{AD-KO}$) *Nos2* knockout mice by crossing homozygous *Nos2*$^{fl/fl}$ mice containing a floxed exon2 with adiponectin-Cre (Adipoq-Cre) mice, respectively (Figure 1A). *Nos2*$^{fl/fl}$ and *Nos2*$^{AD-KO}$ animals were born at the expected Mendelian ratio with no morphological differences. To assess the specificity of the adiponectin-Cre driven recombination of the *Nos2* floxed alleles, genomic DNA was isolated from different tissues. The site of recombination on the *Nos2* gene was mapped, and adiponectin-Cre driven excision of exon2 was confirmed (Figure 1A). Finally, we tested the specificity of the deletion by comparing the rate of *Nos2* exon 2 recombination in different adipose tissues, liver and skeletal muscle. We observed the deleted *Nos2* (Δ*Nos2*) alleles in all white and brown adipose tissue depots of *Nos2*$^{AD-KO}$ animals but not in muscle and liver (Figure 1B) demonstrating that *Nos2* deletion is efficiently working and specific for adipose tissue. Isolation of adipose cells from eWAT, iWAT, and BAT of saline-and LPS-injected mice were also performed to demonstrate a marked reduction of LPS-induced *Nos2* expression in white and brown adipocytes from *Nos2*$^{AD-KO}$ mice (Figure 1C—E).

Adipocyte-selective *Nos2* knockout did not impact normal adipose tissue function. Indeed, we found no change in the plasma levels of adiponectin and leptin, two key adipokines. No genotypic differences were observed for body composition, iWAT, eWAT and BAT histology in mice that were fed regular chow before the start of the dietary intervention (Supplementary Fig. 1).

Nos2^{AD-KO} mice were not protected from HFHS-diet induced obesity, gained the same amount of weight, and had similar energy intake as compared to their littermate controls (Figure 2A,B). The weight of white fat masses as well as other tissues were not different between *Nos2*$^{AD-KO}$ and *Nos2*$^{fl/fl}$ mice (Supplementary Table 1). Interestingly, BAT weight was significantly lower in HFHS-fed *Nos2*$^{AD-KO}$ mice as compared to HFHS-fed *Nos2*$^{fl/fl}$ mice (Figure 2C). *Nos2* expression was significantly reduced in BAT of HFHS fed *Nos2*$^{AD-KO}$ mice, but not in visceral and subcutaneous adipose tissue (Figure 2D—F). The residual *Nos2* expression in adipose tissue from *Nos2*$^{AD-KO}$ mice may represent its undeleted enzyme expression in macrophages and other immune cells, which are the predominant cellular sites of *Nos2* expression in adipose tissue [12]. Accordingly, NOS2 deletion in adipocytes did not affect the typical inflammatory features of epididymal and brown adipose tissues in obese mice, as revealed by the lack of changes in *Adgre1* expression (encoding the F4/80 antigen) as well as M1 and M2 activation markers between HFHS-fed *Nos2*$^{AD-KO}$ and *Nos2*$^{fl/fl}$ mice (Supplementary Figs. 2A and C). On the other hand, we found a tendency for increased *Adgre1* expression in iWAT of *Nos2*$^{AD-KO}$ mice on HFHS diet compared to *Nos2*$^{fl/fl}$ mice (Supplementary Fig. 2B), suggesting a partial compensatory increase in macrophage infiltration in this fat depot in mice lacking adipocyte NOS2.

3.2. HFHS-fed *Nos2*$^{AD-KO}$ mice showed increased insulin sensitivity and reduced plasma triglycerides

We next determined the impact of adipocyte-specific NOS2 disruption on whole body glucose homeostasis. Fasting blood glucose and C-peptide were not different, but fasting insulinemia was reduced in HFHS-fed *Nos2*$^{AD-KO}$ as compared to HFHS *Nos2*$^{fl/fl}$ littermates (Figure 3A—C). Oral glucose tolerance tests (oGTT) showed similar glucose excursion curves between *Nos2*$^{AD-KO}$ and HFHS *Nos2*$^{fl/fl}$mice on either diets (Figure. 3D). However, glucose-stimulated insulin response during the oGTT was significantly improved in HFHS-fed *Nos2*$^{AD-KO}$ mice *versus* HFHS-fed *Nos2*$^{fl/fl}$ further suggesting that adipocyte NOS2 disruption improved insulin sensitivity in obese animals (Figure 3E). C-peptide release was slightly different at 15 min between the HFHS fed groups although there was no significant difference in C-peptide secretion from 30 to 120 min when the insulin responses were markedly different between the genotypes (Figure 3E—F). This suggests that the reduced insulin levels in *Nos2*$^{AD-KO}$ mice on HFHS diet demonstrate an improvement in insulin sensitivity in these mice and/or higher insulin clearance. The improvement of insulin sensitivity was more directly confirmed by the finding of improved insulin tolerance in HFHS fed *Nos2*$^{AD-KO}$ mice compared to their HFHS-fed *Nos2*$^{fl/fl}$ counterparts (Figure 3G).

HFHS-fed *Nos2*$^{AD-KO}$ mice also exhibited an improved lipid profile as compared to HFHS-fed *Nos2*$^{fl/fl}$ controls as revealed by reduced plasma levels of triglycerides, cholesterol, and non-esterified fatty acids (Figure 4A—C). Plasma glycerol levels were also reduced by adipocyte NOS2 ablation but only reached statistical significance in the chow-fed animals (Figure 4D). TG levels in inguinal adipose tissue were increased in *Nos2*$^{AD-KO}$ mice on both diets compared to their littermate controls (Figure 4E), but no genotypic differences were observed in epididymal adipose tissue (Figure 4F). These results together with lower levels of NEFA and a slight reduction in glycerol levels might suggest reduced lipolysis in iWAT. Importantly, neither insulin sensitivity nor plasma TG levels or tissue weights in HFHS-fed mice were affected by adipoq-Cre expression *per se* (see Supplementary Fig. S3 and Supplementary Table 2) validating that the metabolic benefits seen in HFHS-fed *Nos2*$^{AD-KO}$ mice are directly related to selective NOS2 ablation in adipocytes.

3.3. Adipocyte-specific *Nos2* ablation increases energy expenditure and BAT activation in HFHS-fed mice

Indirect calorimetry measurements in metabolic cages revealed reduced oxygen consumption in HFHS-fed *Nos2*$^{fl/fl}$ as compared to the chow-fed counterparts, but this altered phenotype was fully restored in HFHS-fed *Nos2*$^{AD-KO}$ mice (Figure 5A) suggesting that adipose tissue NOS2 is responsible for reduced energy expenditure in obese animals. No differences were observed in CO_2 production, ambulatory movements or the respiratory exchange ratio between HFHS-fed *Nos2*$^{AD-KO}$ and HFHS-fed *Nos2*$^{fl/fl}$ mice (Figure 5B—D).

Given the changes in energy expenditure and reduction of BAT weight suggesting the activation of the tissue in HFHS-fed *Nos2*$^{AD-KO}$ mice, we next sought to further investigate the potential role of BAT function in improved insulin sensitivity and lipid homeostasis in this model. Remarkably, we found that adipocyte *Nos2* ablation markedly raised uncoupling protein-1 (*Ucp1*) expression in BAT of HFHS-fed mice (Figure 6A). We also found a similar increased *Ucp2* expression in BAT of HFHS-fed *Nos2*$^{AD-KO}$ mice compared with HFHS-fed *Nos2*$^{fl/fl}$ mice.

 © 2022 The Authors. Published by Elsevier GmbH. This is an open access article under the CC BY-NC-ND license (http://creativecommons.org/licenses/by-nc-nd/4.0/).

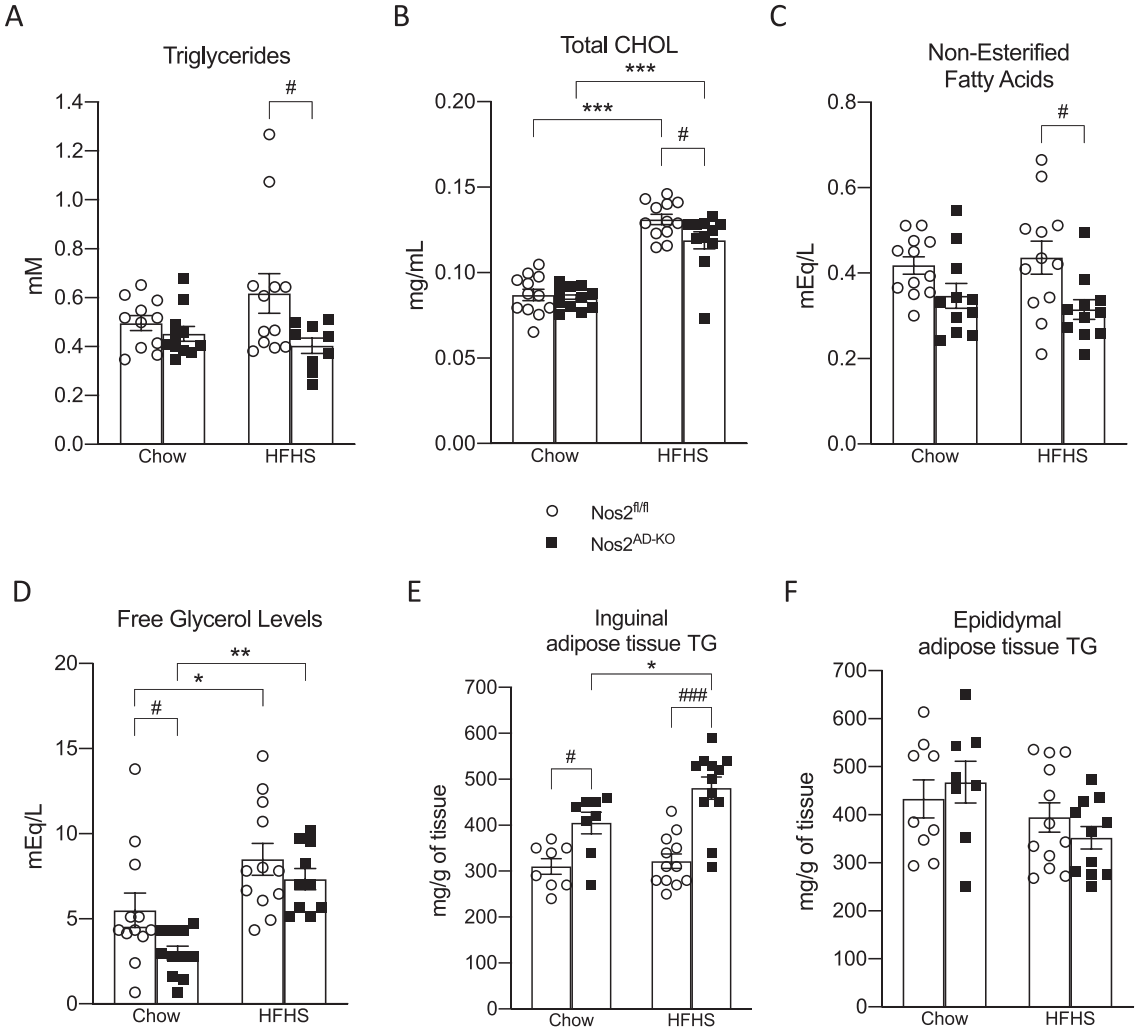

Figure 4: Adipocyte-specific knockout of *Nos2* prevents triglycerides, cholesterol, non-esterified fatty acid and glycerol in plasma. Plasma levels of triglycerides (A), total cholesterol (B) non-esterified fatty acids (C) and free glycerol (D). Adipose tissue triglycerides accumulation in inguinal and epididymal adipose tissue (E,F). Two-way ANOVA with a Student-Newman-Keuls post hoc test was applied to calculate the significance of the differences between groups. Data are expressed as the mean ± SEM. n = 11–12 (B,C); n = 10–12 (A,D); n = 8–12 (E,F); $^{*}p < 0.05$, $^{**}p < 0.01$ and $^{***}p < 0.001$ for diet effect; $^{\#}p < 0.05$ for genotype difference.

Expression of other genes implicated in energy metabolism in BAT such as peroxisome proliferator-activated receptor alpha (*Ppara*), thermogenic gene type II iodothyronine deiodinase (*Dio2*), G-protein coupled bile acid receptor 1 (*Gpbar1*) and peroxisome proliferative activated receptor, gamma, coactivator 1-alpha (*Ppargc1a*) were not affected by *Nos2* deletion (Figure 6A). Total mitochondrial expression of OXPHOS complexes was higher in BAT of HFHS-fed *Nos2*$^{AD-KO}$ mice compared to their HFHS-fed *Nos2*$^{fl/fl}$ littermates (Figure 6C) and these differences were related to specific increases in the levels of complexes II, III and V (Figure 6B). Interestingly, the gene expression of lipoprotein lipase (*Lpl*), a key enzyme controlling the hydrolysis of TG-rich particles, increased in *Nos2*$^{AD-KO}$ animals suggesting a rise in free fatty acid (FFA) delivery to BAT, also consistent with the down-regulation of angiopoietin-like 4 (*Angptl4*) in BAT of HFHS-fed *Nos2*$^{AD-KO}$ as compared to HFHS-fed *Nos2*$^{fl/fl}$ mice (Figure 6D). We also examined whether *Nos2* ablation may induce browning of white adipose tissues. While no changes were observed in inguinal fat (Figure 7A), we found that *Nos2* deletion in adipocytes reduced *Lpl* expression in epididymal fat, which reached the level of significance in chow-fed animals (Figure 7B). However, unlike the findings in BAT, no changes were observed in the expression of *Angptl4* in visceral fat of HFHS-fed *Nos2*$^{AD-KO}$ and HFHS-fed *Nos2*$^{fl/fl}$ mice.

3.4. Nitric oxide directly impairs mitochondrial oxygen consumption in brown adipose cells

To confirm that NOS2 controls BAT thermogenesis, we next used T37i brown adipocytes in culture to investigate whether NOS2 induction directly modulates mitochondrial function in these cells using the Seahorse system. NOS2 expression was induced by incubating brown adipocytes with cytokines as previously described [15]. NOS2 activation and NO production was confirmed by accumulation of nitrite production during cytokine exposure and was completely blocked when using the selective NOS2 inhibitor 1400W (Figure 8A). Seahorse analysis revealed that oxygen consumption rate (OCR) was strongly decreased by cytokine treatment as compared to untreated cells but that selective inhibition of NOS2 activity with 1400W completely reversed the defective mitochondrial respiration (Figure 8B). Addition of different doses of the NO donor SNP confirmed that exogenous NO

 © 2022 The Authors. Published by Elsevier GmbH. This is an open access article under the CC BY-NC-ND license (http://creativecommons.org/licenses/by-nc-nd/4.0/).

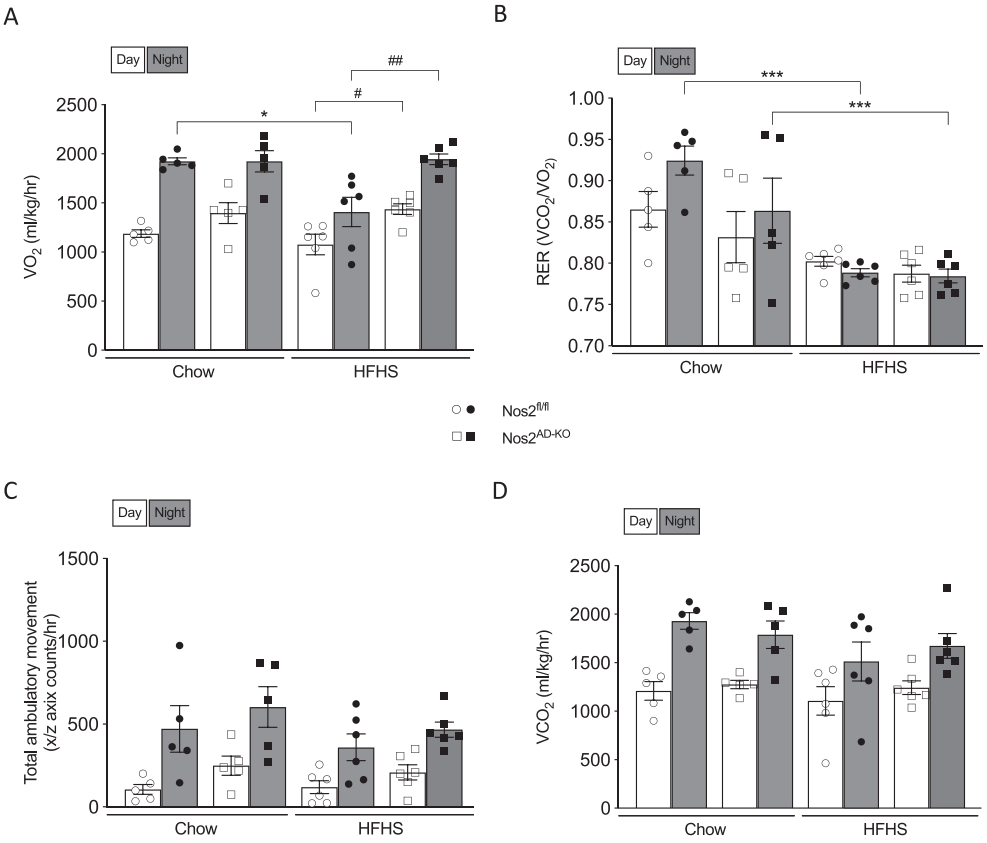

Figure 5: Adipocyte-specific knockout of *Nos2* increases oxygen consumtion in HFHS-fed mice. Oxygen consumption (A), respiratory exchange ratio (B), total ambulatory movement (C) and carbon dioxide production (D) were measured by indirect calorimetry. Two-way ANOVA with a Student-Newman-Keuls post hoc test was applied to calculate the significance of the differences between groups. Data are expressed as the mean ± SEM. n = 9–12 (A,F), n = 5–6 (B,C), n = 10–12 (D,E). $^{*}p < 0.05$ and $^{***}p < 0.001$ for diet effect; $^{\#}p < 0.05$ and $^{\#\#}p < 0.01$ for genotype difference.

reduced OCR (Figure 8C). These results confirm that NOS2 is a cell-autonomous regulator of mitochondrial respiration in BAT, thus providing evidence that NOS2 ablation in BAT is a key mechanism underlying improved energy expenditure in HFHS-fed *Nos2*$^{AD-KO}$ mice.

4. DISCUSSION

We have previously shown that whole body *Nos2* deletion protects mice from high-fat diet-induced insulin resistance [8]. Nevertheless, the target tissue mediating the beneficial effects of NOS2 has not yet been identified. Here, we evaluated the metabolic effects of a specific disruption of *Nos2* in adipose tissue of chow- and HFHS- fed mice. Adipocyte *Nos2* disruption improved HFHS-induced insulin resistance and dyslipidemia. These effects, which were independent of the changes in body weight gain, were accompanied by a decrease in fat accumulation in BAT and a rise in *Ucp1* expression and oxygen consumption in BAT. NOS2 induction in BAT cells impaired oxygen consumption, which was completely restored when NOS2 activity was inhibited, but mimicked by exogenous NO addition.

We and others have demonstrated the effect of whole body *Nos2* deletion in obese and lean mice using different mouse models [8,10,13,16–20]. Importantly, improvement in insulin sensitivity was observed in whole body *Nos2* KO mice treated for 12–18 weeks with HFD [10,20] or in obese *ob/ob* mice lacking *Nos2* [21]. Whole body *Nos2* KO mice are also protected from insulin resistance during lipid infusion as compared to wild-type mice [4]. Pharmacologic inhibition of NOS2 using L-NIL also improved fasting hyperglycemia and improved insulin sensitivity in obese diabetic ob/ob mice [18]. Although induction of NOS2 expression is highest in macrophages, Lu et al. [13] showed that specific *Nos2* ablation in myeloid cells did not protect from insulin resistance, suggesting that non-myeloid cells or tissues are responsible for the beneficial effects of *Nos2* invalidation on insulin sensitivity. The present study reveals a key role of adipocyte NOS2 in mediating insulin resistance and some metabolic alterations in obesity since specific ablation of *Nos2* in adipocytes is sufficient to ameliorate insulin sensitivity as well as the lipid profile. However, some reported effects of systemic NOS2 deletion were not observed in *Nos2*$^{AD-KO}$ mice. In addition to modulating insulin sensitivity, we have reported that whole-body invalidation of *Nos2* in mice led to hyperphagia [8], which was not observed in the current study, suggesting that NOS2 in the central nervous system or other tissues may control food intake.

One major finding of this study is that NOS2 in BAT plays a key role in metabolic homeostasis. Brown adipose tissue is a unique organ that uses UCP1 to uncouple oxidative phosphorylation from ATP production to produce heat. The discovery of a functional BAT in human has greatly contributed to stimulate the interest in this tissue over the last decade.

Even though most human brown fat depots disappear after infancy, a recent study using PET-scan has shown that these fat depots amount for 1.5% of total body mass corresponding to 4.3% of total fat mass. More importantly, up to 90% of human adult BAT could be activated BAT [22]. Also, the function of UCP1 in mitochondria of BAT in human

 © 2022 The Authors. Published by Elsevier GmbH. This is an open access article under the CC BY-NC-ND license (http://creativecommons.org/licenses/by-nc-nd/4.0/).

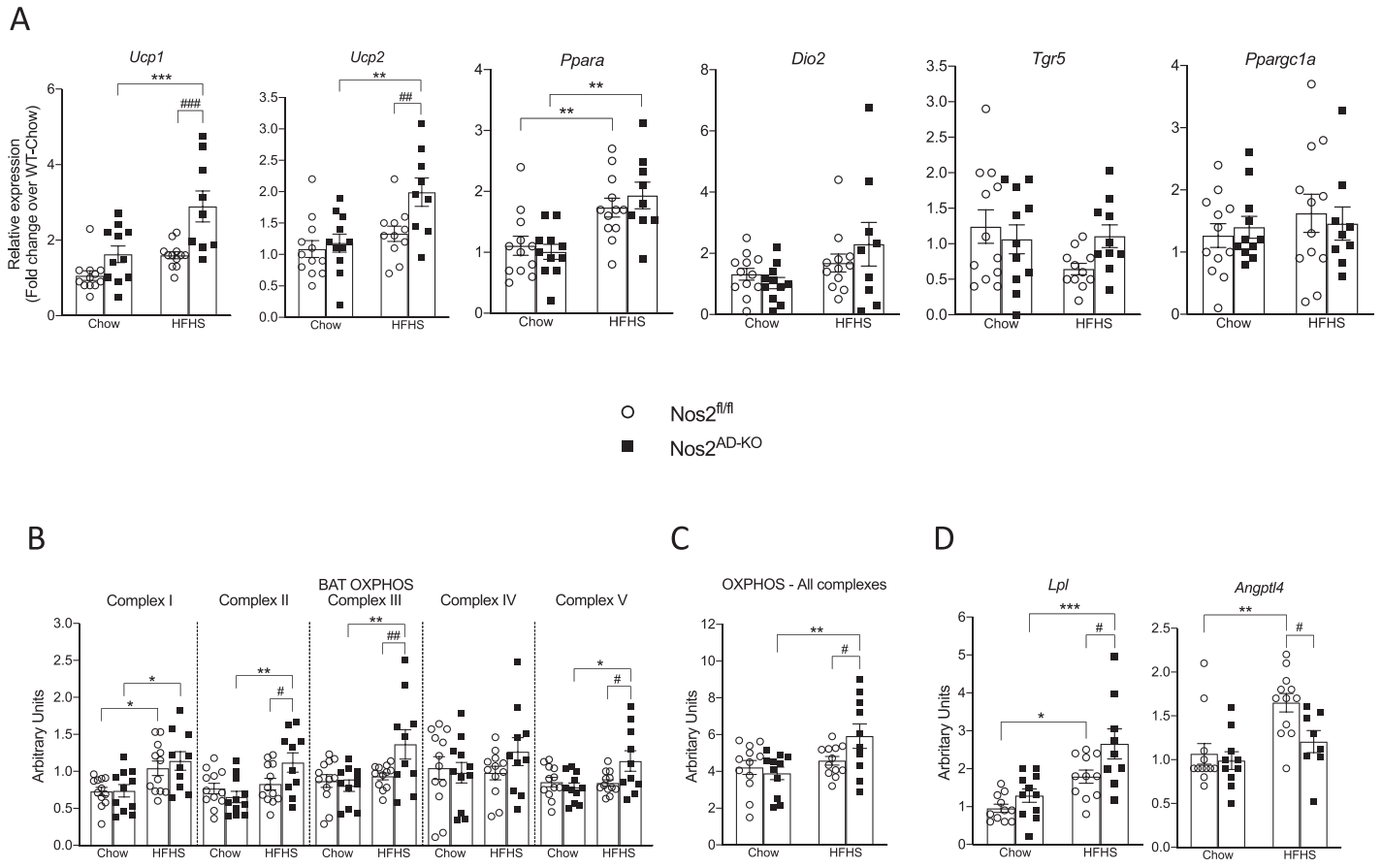

Figure 6: Adipocyte-specific knockout of *Nos2* increases BAT activation in HFHS-fed mice. BAT mRNA expression of genes related to energy metabolism: uncoupling protein 1 (*Ucp1*), uncoupling protein 2 (*Ucp2*), peroxisome proliferator-activated receptor alpha (*Ppara*), type 2 iodothyronine deiodinase (*Dio2*), G-coupled protein receptor (*Tgr5*) and peroxisome proliferator-activated receptor-gamma coactivator (*Ppargc1a*) (A). Protein expression of total OXPHOS complexes (B) and complexes I-IV (C) in BAT. BAT mRNA expression of genes related to lipid metabolism: Lipoprotein lipase (*Lpl*) and Fasting-induced adipose factor/Angiopoietin-like 4 (*Angptl4*) (D). Two-way ANOVA with a Student-Newman-Keuls post hoc test was applied to calculate the significance of the differences between groups. Data are expressed as mean ± SEM. n = 9–12. $^{*}p < 0.05$, $^{**}p < 0.01$ and $^{***}p < 0.001$ for diet effect; $^{\#}p < 0.05$, $^{\#\#}p < 0.01$ and $^{\#\#}p < 0.001$ for genotype difference.

MOLECULAR METABOLISM

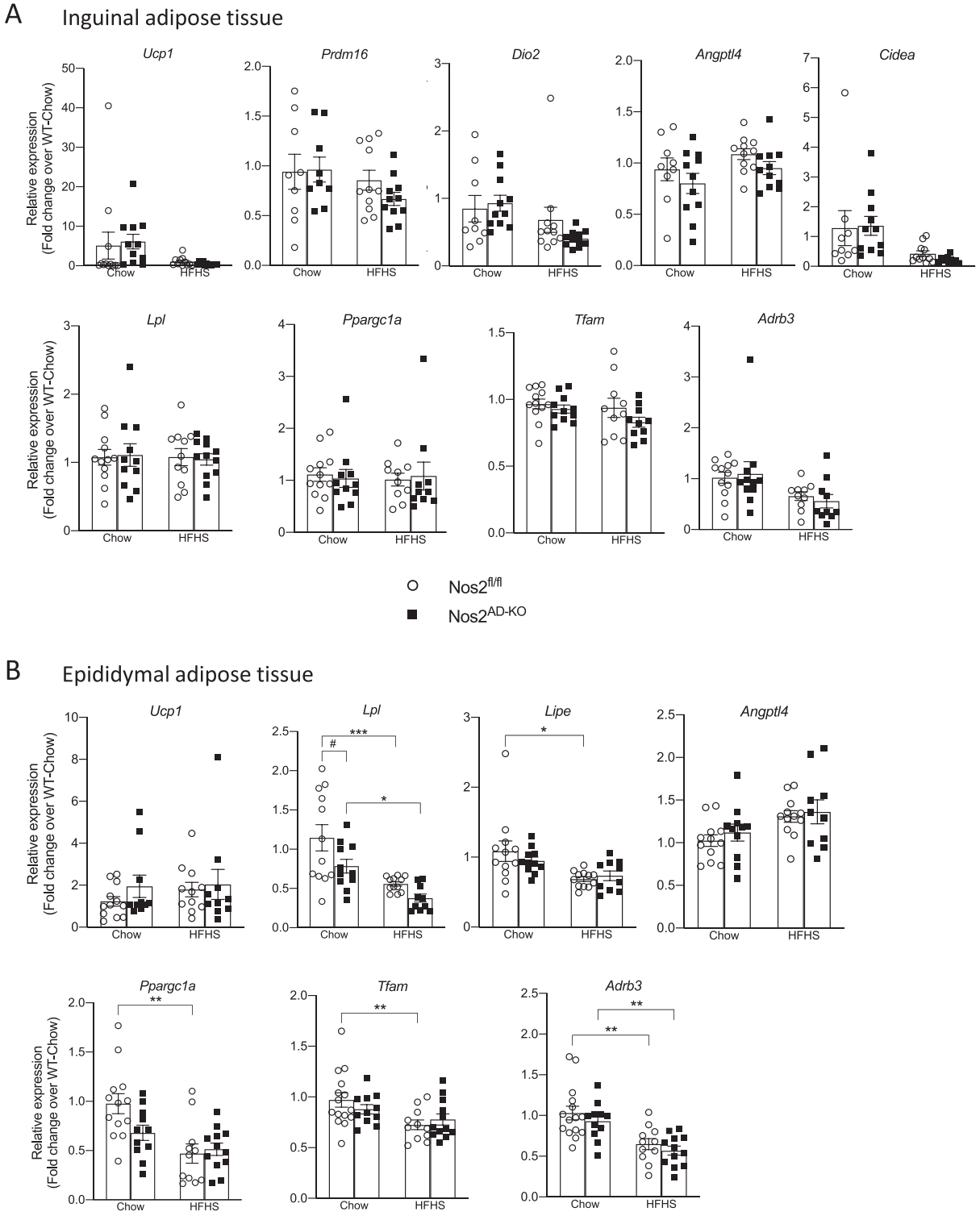

Figure 7: *Nos2* ablation did not change the expression of genes related to browning effect. Genes expressed in energy metabolism, lipid handling and browning in subcutaneous (A) and visceral adipose tissue (B). Tissues were extracted from *Nos2*$^{AD-KO}$ and wild-type (*Nos2*$^{fl/fl}$) mice after 6 h of fasting during sacrifice. Two-way ANOVA with a Student-Newman-Keuls post hoc test was applied to calculate the significance of the differences between groups. Data are expressed as the mean ± SEM. n = 9–12. $^{*}p < 0.05$ and $^{***}p < 0.001$ for diet effect; $^{\#}p < 0.05$ for genotype difference.

 © 2022 The Authors. Published by Elsevier GmbH. This is an open access article under the CC BY-NC-ND license (http://creativecommons.org/licenses/by-nc-nd/4.0/).

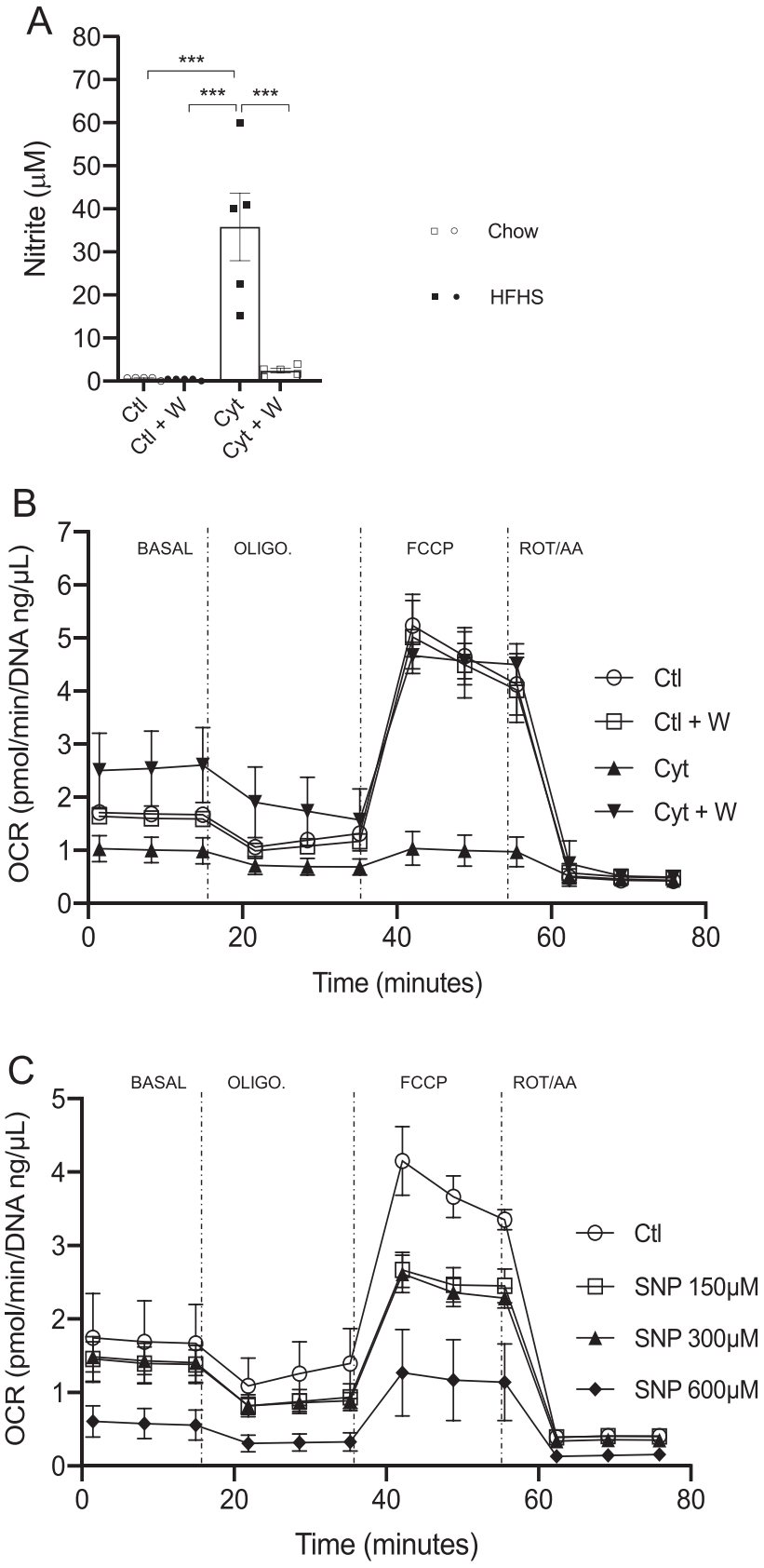

Figure 8: Nitric oxide affects oxygen consumption in brown adipose cells. Differentiated T37i cells were exposed to cytokine cocktail with or without 1400W (100 μM) for 24 h. Nitrite was determined in the supernatant (A) and oxygen consumption rate (OCR) was determined by running the Seahorse mitostress protocol (B). T37i cells were exposed to different concentrations of sodium nitroprusside (SNP) for 16 h and OCR was determined as in B (C). Data are expressed as the mean ± SEM. n = 3 (A, B); n = 2 (C).

 © 2022 The Authors. Published by Elsevier GmbH. This is an open access article under the CC BY-NC-ND license (http://creativecommons.org/licenses/by-nc-nd/4.0/).

and mouse is comparable [23], highlighting the importance of studies using mouse models. We found a robust increase in *Ucp1* gene expression in BAT of *Nos2*$^{AD-KO}$ mice. Becerril and colleagues [21] also showed UCP1 activation in whole body *Nos2* KO mice although they also observed a reduction in food intake, which is a potential confounding factor. It is known that increased BAT thermogenesis is tightly correlated with increased UCP1 expression in BAT [24]. Interestingly, *Nos2* deletion in brown adipocytes also increased *Ucp2* gene expression in BAT of *Nos2*$^{AD-KO}$ mice, which could also be involved in both, the raised energy expenditure and improved lipid profile of these mice. Indeed, UCP2 is also involved in cold-induced BAT thermogenesis [25] whereas the lack of UCP2 also led to higher TG concentration in BAT favoring glucose utilization [25]. It has also been shown that BAT takes up plasma TG via lipolysis [26,27], which is well aligned with the increase in *Lpl* expression we have observed here and the reduction in plasma TG, which is also in accordance with the effect of adipocyte *Nos2* ablation on *Angptl4*, a well known LPL inhibitor. Although BAT activation in mice lacking adipocyte NOS2 was associated with increased energy expenditure and improved glucose and lipid metabolism within 7—10 weeks of dietary treatments, we did not observe body weight reduction in *Nos2*$^{AD-KO}$ mice as compared to their WT floxed littermates. It is possible that longer term changes in BAT thermogenesis and energy metabolism are needed to translate into significant body weight change in mice. This is supported by the previous findings that BAT transplantation improves glucose homeostasis and insulin sensitivity within 8 weeks, but that body weight changes became only significant after 12 weeks in these mice [28].

Further analysis of BAT in our study also points toward the role of NOS2 in regulating mitochondrial capacity of brown adipocytes in *Nos2*$^{AD-KO}$ mice, as indicated by increased levels of mitochondrial complex II, III, and IV protein expression, which suggests more demand for these complexes in the absence of NOS2 in BAT. This mechanism was confirmed using T37i brown fat cells whereby NOS2 induction was shown to directly impair mitochondrial respiration, and it was completely reversed by inhibiting NOS2 activity. Moreover, direct addition of exogenous NO dose dependently impaired oxygen consumption rate in these cells, demonstrating that NOS2-derived NO is a cell-autonomous negative modulator of BAT mitochondria. This is consistent with the previous studies using various cell types or isolated mitochondria showing that NO can inhibit mitochondrial respiration acting on complex I and IV [29—32]. A recent study by Sebag et al. has shown that UCP1 has a S-nitrosylation site (Cys305) dampening its activity. High-fat feeding led to an increase in NO-mediated S-nitrosylation of this site and loss of the denitrosylase alcohol dehydrogenase 5 (ADH5), which balances the nitroso-redox status in BAT, caused impaired UCP1 dependent thermogenesis [33]. Other potential mechanisms that are worth pursuing in follow-up studies are potential changes in mitochondrial fission, which is known to be raised by β-adrenergic activation of BAT thermogenesis [34], and may involve a key role for mitofusin 2 based on the finding that mitofusin 2 ablation in BAT improves insulin sensitivity in mice fed a high-fat diet [35]. Finally, NO can directly inhibit cytochrome oxidase (complex IV) whereas the potent NO-derived radical peroxynitrite can inhibit multiple respiratory complexes (complexes I-IV) [36]. It is therefore conceivable that reduced peroxynitrite formation may be involved in promoting changes in the mitochondrial respiratory chain in brown adipocytes lacking *Nos2*.

Overall, our results demonstrate that targeted ablation of *Nos2* in adipocytes *in vivo* protects against obesity-linked insulin resistance. This effect was associated with improved lipid profile and raised energy expenditure that is linked to BAT activation, which we have mechanistically related to reduced NO-dependent inhibition of mitochondrial respiration. Our results thus identify adipose NOS2 as an important player in obesity-related metabolic diseases at least in part by impeding BAT thermogenesis through NO-mediated inhibition of mitochondrial oxidative metabolism.

CONFLICT OF INTEREST

The authors declare no competing financial interests. AM has been the holder of Pfizer/CIHR partnered research chair and received grants from Danone Nutricia Research, Acasti Pharma, Allysta inc. None of these funding sources are relevant to this publication. No other potential dualities of interest are associated with this article.

ACKNOWLEDGMENTS

We thank Patricia L. Mitchell for assisting with the statistical analysis.

A.M., M.L., V.R.V. and K.B. conceived and planned the study. V.R.V, R.N. and G.L. conducted the animal experiments and did the data analysis together with N.S., L.R.P., C.C.B., V.R and P.Z. V.R.V, N.S. and R.N. generated the figures. V.R.V., N.S., R.N. and L.R.P. integrated the data. V.R.V., A.M., M.L. and K.B. wrote the manuscript. V.R.V, N.S., R.N, V.R., L.R.P., G.L., C.C.B., P.Z., M.S.P., K.B., V.D., M.L. and A.M. contributed to data analysis and discussion and agreed upon the submitted manuscript.

This study was supported by a Canadian Institutes of Health Research (CIHR) Foundation Scheme grant to A.M. (FDN 143247) and the Canada Excellence Research Chair on the Microbiome—Endocannabinoidome Axis in Metabolic Health (CERC-MEND), which is supported by a Canadian Federal Tri-Agency grant (to V.D.).

APPENDIX A. SUPPLEMENTARY DATA

Supplementary data to this article can be found online at https://doi.org/10.1016/j.molmet.2022.101437.

REFERENCES

[1] Moncada, S., Palmer, R.M., Higgs, E.A., 1991. Nitric oxide: physiology, pathophysiology, and pharmacology. Pharmacological Reviews 43(2):109—142.

[2] Nathan, C., 1997. Inducible nitric oxide synthase: what difference does it make? Journal of Clinical Investigation 100(10):2417—2423.

[3] Beckman, J.S., Koppenol, W.H., 1996. Nitric oxide, superoxide, and peroxynitrite: the good, the bad, and ugly. American Journal of Physiology 271(5 Pt 1):C1424—C1437.

[4] Charbonneau, A., Marette, A., 2010. Inducible nitric oxide synthase induction underlies lipid-induced hepatic insulin resistance in mice: potential role of tyrosine nitration of insulin signaling proteins. Diabetes 59(4):861—871.

[5] Morris, B.J., Markus, A., Glenn, C.L., Adams, D.J., Colagiuri, S., Wang, L., 2002. Association of a functional inducible nitric oxide synthase promoter variant with complications in type 2 diabetes. Journal of Molecular Medicine (Berlin) 80(2):96—104.

[6] Torres, S.H., De Sanctis, J.B., de, L.B.M., Hernandez, N., Finol, H.J., 2004. Inflammation and nitric oxide production in skeletal muscle of type 2 diabetic patients. Journal of Endocrinology 181(3):419—427.

[7] Carvalho-Filho, M.A., Ueno, M., Hirabara, S.M., Seabra, A.B., Carvalheira, J.B., de Oliveira, M.G., et al., 2005. S-nitrosation of the insulin receptor, insulin receptor substrate 1, and protein kinase B/Akt: a novel mechanism of insulin resistance. Diabetes 54(4):959—967.

[8] Perreault, M., Marette, A., 2001. Targeted disruption of inducible nitric oxide synthase protects against obesity-linked insulin resistance in muscle. Nature Medicine 7(10):1138—1143.

 © 2022 The Authors. Published by Elsevier GmbH. This is an open access article under the CC BY-NC-ND license (http://creativecommons.org/licenses/by-nc-nd/4.0/).

[9] Pilon, G., Charbonneau, A., White, P.J., Dallaire, P., Perreault, M., Kapur, S., et al., 2010. Endotoxin mediated-iNOS induction causes insulin resistance via ONOO(-) induced tyrosine nitration of IRS-1 in skeletal muscle. PLoS One 5(12):e15912.

[10] Dallaire, P., Bellmann, K., Laplante, M., Gelinas, S., Centeno-Baez, C., Penfornis, P., et al., 2008. Obese mice lacking inducible nitric oxide synthase are sensitized to the metabolic actions of peroxisome proliferator-activated receptor-gamma agonism. Diabetes 57(8):1999—2011.

[11] Yasukawa, T., Tokunaga, E., Ota, H., Sugita, H., Martyn, J.A., Kaneki, M., 2005. S-nitrosylation-dependent inactivation of Akt/protein kinase B in insulin resistance. Journal of Biological Chemistry 280(9):7511—7518.

[12] Weisberg, S.P., McCann, D., Desai, M., Rosenbaum, M., Leibel, R.L., Ferrante Jr., A.W., 2003. Obesity is associated with macrophage accumulation in adipose tissue. Journal of Clinical Investigation 112(12):1796—1808.

[13] Lu, M., Li, P., Pferdekamper, J., Fan, W., Saberi, M., Schenk, S., et al., 2010. Inducible nitric oxide synthase deficiency in myeloid cells does not prevent diet-induced insulin resistance. Molecular Endocrinology 24(7):1413—1422.

[14] Rao, A.M., Dogan, A., Hatcher, J.F., Dempsey, R.J., 1998. Fluorometric assay of nitrite and nitrate in brain tissue after traumatic brain injury and cerebral ischemia. Brain Research 793(1—2):265—270.

[15] Penfornis, P., Marette, A., 2005. Inducible nitric oxide synthase modulates lipolysis in adipocytes. The Journal of Lipid Research 46(1):135—142.

[16] Becerril, S., Rodriguez, A., Catalan, V., Sainz, N., Ramirez, B., Collantes, M., et al., 2010. Deletion of inducible nitric-oxide synthase in leptin-deficient mice improves brown adipose tissue function. PLoS One 5(6):e10962.

[17] Cha, H.N., Song, S.E., Kim, Y.W., Kim, J.Y., Won, K.C., Park, S.Y., 2011. Lack of inducible nitric oxide synthase prevents lipid-induced skeletal muscle insulin resistance without attenuating cytokine level. Journal of Pharmacological Sciences 117(2):77—86.

[18] Fujimoto, M., Shimizu, N., Kunii, K., Martyn, J.A., Ueki, K., Kaneki, M., 2005. A role for iNOS in fasting hyperglycemia and impaired insulin signaling in the liver of obese diabetic mice. Diabetes 54(5):1340—1348.

[19] Kanuri, B.N., Kanshana, J.S., Rebello, S.C., Pathak, P., Gupta, A.P., Gayen, J.R., et al., 2017. Altered glucose and lipid homeostasis in liver and adipose tissue pre-dispose inducible NOS knockout mice to insulin resistance. Scientific Reports 7:41009.

[20] Zanotto, T.M., Quaresma, P.G.F., Guadagnini, D., Weissmann, L., Santos, A.C., Vecina, J.F., et al., 2017. Blocking iNOS and endoplasmic reticulum stress synergistically improves insulin resistance in mice. Molecular Metabolism 6(2): 206—218.

[21] Becerril, S., Rodriguez, A., Catalan, V., Mendez-Gimenez, L., Ramirez, B., Sainz, N., et al., 2018. Targeted disruption of the iNOS gene improves adipose tissue inflammation and fibrosis in leptin-deficient ob/ob mice: role of tenascin C. International Journal of Obesity 42(8):1458—1470.

[22] Leitner, B.P., Huang, S., Brychta, R.J., Duckworth, C.J., Baskin, A.S., McGehee, S., et al., 2017. Mapping of human brown adipose tissue in lean and obese young men. Proceedings of the National Academy of Sciences of the United States of America 114(32):8649—8654.

[23] Porter, C., Herndon, D.N., Chondronikola, M., Chao, T., Annamalai, P., Bhattarai, N., et al., 2016. Human and mouse Brown adipose tissue mitochondria have comparable UCP1 function. Cell Metabolism 24(2):246—255.

[24] Koban, M., Swinson, K.L., 2005. Chronic REM-sleep deprivation of rats elevates metabolic rate and increases UCP1 gene expression in brown adipose tissue. American Journal of Physiology. Endocrinology and Metabolism 289(1): E68—E74.

[25] Caron, A., Labbe, S.M., Carter, S., Roy, M.C., Lecomte, R., Ricquier, D., et al., 2017. Loss of UCP2 impairs cold-induced non-shivering thermogenesis by promoting a shift toward glucose utilization in brown adipose tissue. Biochimie 134:118—126.

[26] Bartelt, A., Bruns, O.T., Reimer, R., Hohenberg, H., Ittrich, H., Peldschus, K., et al., 2011. Brown adipose tissue activity controls triglyceride clearance. Nature Medicine 17(2):200—205.

[27] Khedoe, P.P., Hoeke, G., Kooijman, S., Dijk, W., Buijs, J.T., Kersten, S., et al., 2015. Brown adipose tissue takes up plasma triglycerides mostly after lipolysis. The Journal of Lipid Research 56(1):51—59.

[28] Stanford, K.I., Middelbeek, R.J., Townsend, K.L., An, D., Nygaard, E.B., Hitchcox, K.M., et al., 2013. Brown adipose tissue regulates glucose homeostasis and insulin sensitivity. Journal of Clinical Investigation 123(1):215—223.

[29] Beltran, B., Quintero, M., Garcia-Zaragoza, E., O'Connor, E., Esplugues, J.V., Moncada, S., 2002. Inhibition of mitochondrial respiration by endogenous nitric oxide: a critical step in Fas signaling. Proceedings of the National Academy of Sciences of the United States of America 99(13):8892—8897.

[30] Clementi, E., Brown, G.C., Feelisch, M., Moncada, S., 1998. Persistent inhibition of cell respiration by nitric oxide: crucial role of S-nitrosylation of mitochondrial complex I and protective action of glutathione. Proceedings of the National Academy of Sciences of the United States of America 95(13): 7631—7636.

[31] Koivisto, A., Matthias, A., Bronnikov, G., Nedergaard, J., 1997. Kinetics of the inhibition of mitochondrial respiration by NO. FEBS Letters 417(1):75—80.

[32] Lizasoain, I., Moro, M.A., Knowles, R.G., Darley-Usmar, V., Moncada, S., 1996. Nitric oxide and peroxynitrite exert distinct effects on mitochondrial respiration which are differentially blocked by glutathione or glucose. Biochemical Journal 314(Pt 3):877—880.

[33] Sebag, S.C., Zhang, Z., Qian, Q., Li, M., Zhu, Z., Harata, M., et al., 2021. ADH5-mediated NO bioactivity maintains metabolic homeostasis in brown adipose tissue. Cell Reports 37(7):110003.

[34] Wikstrom, J.D., Mahdaviani, K., Liesa, M., Sereda, S.B., Si, Y., Las, G., et al., 2014. Hormone-induced mitochondrial fission is utilized by brown adipocytes as an amplification pathway for energy expenditure. The EMBO Journal 33(5): 418—436.

[35] Mahdaviani, K., Benador, I.Y., Su, S., Gharakhanian, R.A., Stiles, L., Trudeau, K.M., et al., 2017. Mfn2 deletion in brown adipose tissue protects from insulin resistance and impairs thermogenesis. EMBO Reports 18(7):1123—1138.

[36] Brown, G.C., Borutaite, V., 2002. Nitric oxide inhibition of mitochondrial respiration and its role in cell death. Free Radical Biology and Medicine 33(11): 1440—1450.

 © 2022 The Authors. Published by Elsevier GmbH. This is an open access article under the CC BY-NC-ND license (http://creativecommons.org/licenses/by-nc-nd/4.0/).